Interplay between transition-metal K-edge XMCD, slight structural distortions and magnetism in a series of trimetallic (CoxNi(1– x))4[Fe(CN)6]3/8 Prussian blue analogues

Adama N'Diaye, Amélie Bordage, Lucie Nataf, François Baudelet, Eric Rivière, Anne Bleuzen

ARTICLE

Interplays between transition-metal K-edge XMCD, slight structural distortions and magnetism in a series of trimetallic $(Co_xNi_{(1-x)})_4[Fe(CN)_6]_{3/8}$ Prussian Blue Analogs.

Received 00th January 20xx,
Accepted 00th January 20xx

DOI: 10.1039/x0xx00000x

Adama N'Diaye,[a] Amélie Bordage,[a] Lucie Nataf,[b] François Baudelet,[b] Eric Rivière,[a] and Anne Bleuzen[a]*

The magnetic properties of a series of trimetallic (Co,Ni)Fe Prussian blue analogs (PBA) were investigated by SQUID magnetometry and X-ray Magnetic Circular Dichroism (XMCD) at the three Transition Metals (TM) K-edges. In return the PBA trimetallic series was used as a tool in order to better understand the information contained in TM K-edge XMCD, and particularly the chemical nature of the probed species (extended sub-lattice or localized entities). The results show that the magnetic behavior of the compounds is dictated by the Zeeman effect and competing exchange interactions between the Co-Fe and Ni-Fe pairs, without spin frustration. They also show that XMCD at the TM K-edge is a local atomic probe of the element at the N side of the cyanide bridge and a local probe of the absorbing atom and its first magnetic neighbors on the C side of the bridge. At last, XMCD at the TM K-edge turns out to be highly sensitive to very small structural distortions.

Introduction

X-ray Magnetic Circular Dichroism (XMCD) at the Transition Metals (TM) K-edge is less frequently used than XMCD at the TM $L_{2,3}$ edges as a local magnetic probe. Indeed, in contrast with XMCD at the $L_{2,3}$ edges of TM, for which quantitative information can be extracted from the sum rules[1-3] and the spectra can be well-reproduced by crystal field multiplet calculations,[4] the interpretation of the XMCD signals at the TM K-edge remains unsatisfactory despite many efforts towards their quantitative interpretation and the reproduction of the signals.[5-15] And yet, XMCD at the TM K-edge is the preferred technique to probe magnetism under pressure for instance.[16-21] The literature on XMCD at the TM K-edge mostly deals with the study of metals,[22] metal alloys[23] and intermetallics,[25-26] while works dealing with the study of molecular compounds are scarcer.

Most of the studies of molecular compounds by XMCD at the TM K-edge deals with the investigation of Prussian Blue Analogs (PBAs). Noticeably, in the search for room-temperature molecular-based magnets, Verdaguer and his team used this technique in the 90's as a probe of the exchange interactions in PBAs : they related the sign of the TM K-edge XMCD signal to the orientation of the magnetic moment carried by the absorbing atom with respect to the applied magnetic field.[27-34] Since then, only qualitative information was extracted from these signals.

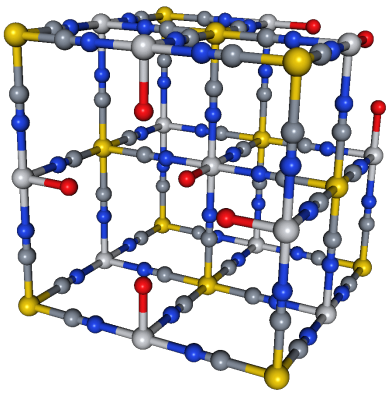

Figure 1. *Scheme of the unit cell of a Prussian blue analog with chemical formula $A_4[B(CN)_6]_{2.7}\bullet xH_2O$. Yellow circles stand for the B^{3+} ion, light grey circles the A^{2+} ions, dark grey the carbon atoms, blue the nitrogen atoms, and red the oxygen atoms. The hydrogen atoms of the water molecules bonded to the A^{2+} ions as well as the zeolitic water molecules are omitted for clarity.*

Therefore, we are engaged in the project aiming at disentangling the physical effects at the origin of the TM K-edge XMCD signals. We have been developing an original experimental approach aiming at making TM K-edge XMCD a real quantitative tool for molecular chemists.[35-39] Our strategy, presented in previous works,[36-39] uses the versatile chemistry of PBAs exhibiting the well-known face-centered cubic (fcc)

[a] *Institut de Chimie Moléculaire et des Matériaux d'Orsay, Université Paris-Saclay, CNRS, 91405 Orsay, France.*
[b] *Synchrotron SOLEIL, L'Orme des Merisiers, St Aubin, BP 48, 91192 Gif sur Yvette, France.*

† Footnotes relating to the title and/or authors should appear here.
Electronic Supplementary Information (ESI) available: [details of any supplementary information available should be included here]. See DOI: 10.1039/x0xx00000x

structure, the unit cell of which is shown in Figure 1 (for p = 4 and q = 8/3) and the chemical composition per unit cell is given by $A_p[B(CN)_6]_q \bullet nH_2O$, where A and B are two TM ions. The large variety of TM ions that can thus be combined in isostructural compounds, allows for the independent variation of the magnetic orbitals on both A and B sites. This affords the analysis of the effect of a change of each of them on both TM K-edges XMCD signals. Thus, the analysis of the TM K-edge XMCD signals of two series of PBAs of chemical formula $A^{II}_4[Fe^{III}(CN)_6]_{3/8} \bullet nH_2O$ (A^{2+} = Mn^{2+}, Co^{2+}, Ni^{2+}, Cu^{2+}) and $A^{II}_4[Cr^{III}(CN)_6]_{3/8} \bullet nH_2O$ (A^{2+} = Mn^{2+}, Fe^{2+}, Co^{2+}, Ni^{2+}) showed that TM K-edge XMCD is very sensitive to orbital symmetry and allowed us to relate the main 1s → 4p contribution of the XMCD signal to the electronic structure and the magnetic behavior of i) the probed ion on the N side of the cyanide bridge and ii) the probed ion and its magnetic neighbors on the C side. Furthermore, an expression for the intensity of this main 1s → 4p contribution was unprecedently derived for the sixteen XMCD signals (at both TM K-edges of the eight PBAs) of the two series.[37, 39] This study also showed that XMCD at the TM K-edge can provide original local, both structural and magnetic information which, combined with macroscopic magnetic measurements, allowed for an unprecedented in-depth analysis of the magnetic behaviors of the two bimetallic series of PBAs.

In this work, we now focus on a series of trimetallic PBAs. Twenty-five years ago, trimetallic PBAs generated interest for their intriguing magnetic behaviors and particularly magnetic pole inversions due to competitive exchange interactions between the TM ions,[40-48] and also, later on, some photo-switching properties;[49-51] their magnetic properties were essentially investigated by SQUID magnetometry at the macroscopic level. In our on-going commitment to promote TM K-edge XMCD as a regular local probe of TM magnetic moment in molecular compounds, these systems offer the opportunity to go ahead. On the one hand, such study of trimetallic PBAs is an opportunity to test the relevancy of TM K-edge XMCD for the study of the magnetic properties of more complex systems than bimetallic PBAs. On the other hand, with the aim to better understand the information contained in the XMCD signals, one can analyze the effect on the XMCD signal at the three TMs K-edges of the replacement of one ion by another in varying amount in the same sublattice of one PBA ; this should provide information on the nature of the species probed (extended on a sublattice level or local at the atomic scale). Among trimetallic PBAs, the series of chemical formula $(Co_xNi_{(1-x)})_4[Fe(CN)_6]_{8/3} \bullet nH_2O$, (where x is the mole fraction of Co ions on the A site of the alkali cation free NiFe PBA), called the **$Co_xNi_{(1-x)}Fe$** series in the following, has been chosen. The preparation of the samples, and their characterizations are given in the experimental part and the supplementary materials (S1-S3).

Results

Magnetic measurements.

The magnetization curves versus the magnetic field at 4 K, temperature at which the XMCD measurements were performed, are shown in Figure 2 for the samples of the **$Co_xNi_{(1-x)}Fe$** series. The Field Cooled (FC) and Zero Field Cooled (ZFC) magnetization curves, as well as the temperature dependence of the inverse of magnetic molar susceptibilities, are given in S2 and S3. The magnetic ordering temperature $T_{C/N}$ was determined as the temperature of a minimum in the derivative of the FC magnetization curve ($dM_{FC}(T)/dT$; S2). The Weiss (θ) magnetic constant was extracted from the plots of the inverse of the molar susceptibility versus temperature by fitting a Curie-Weiss law to the curves (S3). All these magnetic data as well as the coercive field (H_C) at 4 K and the magnetization value at 4 K and 4 T are gathered in Table 1.

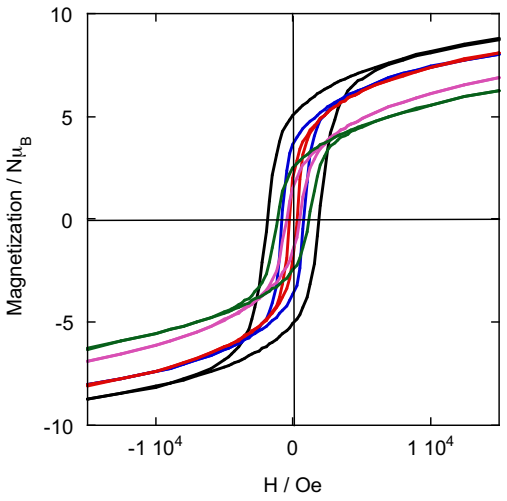

Figure 2. *Magnetic field dependance of the magnetization at 4 K of* ***CoFe*** *(green),* ***$Co_{0.7}Ni_{0.3}Fe$*** *(pink),* ***$Co_{0.56}Ni_{0.44}Fe$*** *(red),* ***$Co_{0.35}Ni_{0.65}Fe$*** *(blue),* ***NiFe*** *(black).*

	$T_{C/N}$ (K)	θ (K)	H_c (x10^{-4} T)	M (4 T) ($N\mu_B$)	$M_{sat\ calc}$ Powder mixture ($N\mu_B$)	$M_{sat\ calc}$ ($N\mu_B$)
CoFe	14	-9	1240	8.3	9.3	9.3
$Co_{0.7}Ni_{0.3}Fe$	12	-0.25	500	8.9	9.7	3.3
$Co_{0.56}Ni_{0.44}Fe$	12	8.3	250	9.7	9.9	0.5
$Co_{0.35}Ni_{0.65}Fe$	16	14	750	9.4	10.2	3.7
NiFe	22	32	2000	10.1	10.7	10.7

Table 1. *Macroscopic magnetic parameters for* ***CoFe, $Co_{0.7}Ni_{0.3}Fe$, $Co_{0.56}Ni_{0.44}Fe$, $Co_{0.35}Ni_{0.65}Fe$, NiFe****.*

The FC/ZFC magnetization curves (S2) exhibit the classical profile of PBA magnets and they show that at 4 K, temperature at which the XMCD signals were recorded, all compounds are in a magnetically ordered state. The single X-ray diffraction peak for each reflection (S1), the unique minimum exhibited by the $dM_{FC}(T)/dT$ curve (S2) and the profile of the magnetic field dependence of the magnetization (Figure 2) show that all compounds are made of a homogeneous PBA phase mixing the Ni^{2+} and Co^{2+} ions at the atomic scale. The presence of several phases richer in one or the other ion can be excluded.

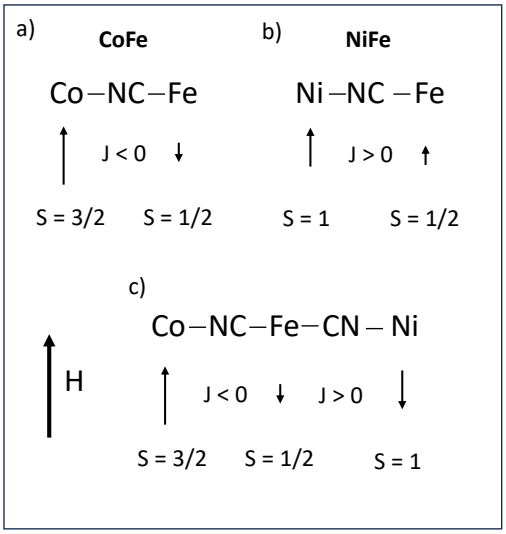

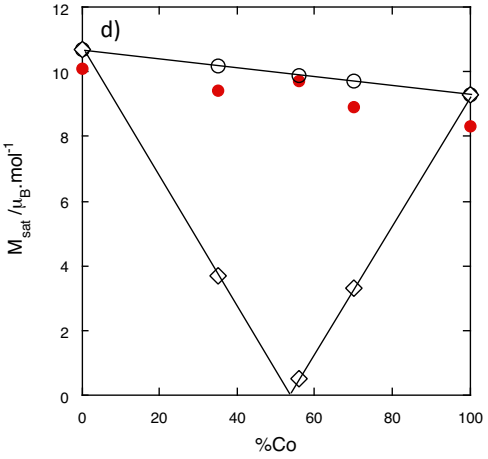

Figure 3. *Scheme of the orientation of the magnetic moment borne by the TM ions in an applied magnetic field H for a)* ***CoFe****, b)* ***NiFe*** *and c) the* ***$Co_xNi_{(1-x)}Fe$*** *series by considering the same magnetic behavior as in the* ***$Mn_xNi_{(1-x)}Cr$*** *series.[40-43] d) Experimental magnetization value at 4 K and 4 T (red circle) for the* ***$Co_xNi_{(1-x)}Fe$*** *series and M_{sat} values as a function of x calculated from Eq. 1 (white diamond) and for the corresponding mixture of the* ***CoFe*** *and* ***NiFe*** *PBA powders (white circle).*

As a first approximation, for TM ions of the first row, magnetic moments are considered originating from the spin angular momentum only. In the magnetically ordered states of PBAs, the orientation of the magnetic moments with regard to an applied external magnetic field can thus generally be predicted from the total spin quantum number of the ions and from the sign of J. In bimetallic PBAs, the magnetic moment of the ion with the largest total spin quantum number aligns in the direction of the magnetic field and the second one is parallel (J>0) or antiparallel (J<0) to the former depending on the sign of J. In such compounds where exchange interactions prevail, the sign of θ directly gives the sign of J. Thus, **CoFe** is a ferrimagnet: the magnetic moment carried by the Co^{2+} ion aligns in the direction of the applied magnetic field and the one of the Fe^{3+} ion in the opposite direction (Figure 3a).[37] In contrast, **NiFe** is a ferromagnet: the magnetic moments carried by the Ni^{2+} and the Fe^{3+} ions align both in the direction of the applied magnetic field (Figure 3b).[37] In trimetallic PBAs containing two different metal ions pairs with different nature of exchange interactions (antiferro- and ferromagnetic) between them, the situation is more complex. As mentioned in the introductory part, several examples of magnetic studies of trimetallic PBAs exist in the literature and especially the PBAs series of chemical formula $(Mn_xNi_{(1-x)})_4[Cr(CN)_6]_{8/3}\bullet nH_2O$[40-43] called **$Mn_xNi_{(1-x)}Cr$** series in the following. This trimetallic PBAs series is comparable to our series as the extreme compounds **MnCr** and **NiCr** are also respectively ferrimagnet and ferromagnet. For this **$Mn_xNi_{(1-x)}Cr$** series the saturation magnetization was well predicted along the series by considering the same exchange interaction as in the extreme bimetallic compounds between the same pairs of ions. In the same way, we tried to predict the saturation magnetization value for one unit cell for the compounds of the **$Co_xNi_{(1-x)}Fe$** series by considering the same exchange interaction as in the bimetallic extreme PBAs between the same ions pairs using Eq. 1 in $N\mu_B$ unit, where N is the Avogadro constant, μ_B the Bohr magneton and g the electron g-factor (g=2) and which is equivalent to the equation used in ref. 40-43:

$$\mathbf{M}_{sat\ calc} = g|4(xS_{Co} - (1-x)S_{Ni}) - 8/3\,S_{Fe}| \qquad (1)$$

The calculated values ($M_{sat\ calc}$) are given in table 1 and plotted as a function of x in Figure 3d, where they are compared to the experimental magnetization values at 4 T and the values calculated for the corresponding mixture of the **CoFe** and **NiFe** PBA powders. Even if the saturation is not reached at 4 T, Figure 3d clearly shows that Eq. 1 fails to predict the experimental saturation magnetization in our **$Co_xNi_{(1-x)}Fe$** series. The magnetic behavior of our **$Co_xNi_{(1-x)}Fe$** series is therefore different from that of the **$Mn_xNi_{(1-x)}Cr$** one described in ref. 40-43. To get a better insight into this original magnetic behavior, the compounds of the **$Co_xNi_{(1-x)}Fe$** series were investigated by XMCD at the Co, Ni and Fe K-edges to probe the local magnetic moment on each TM ion.

XMCD at the Co and Ni K-edges.

The XMCD signals at the Co and Ni K-edges for the **$Co_xNi_{(1-x)}Fe$** series are shown in Figures 4a and 4b respectively.

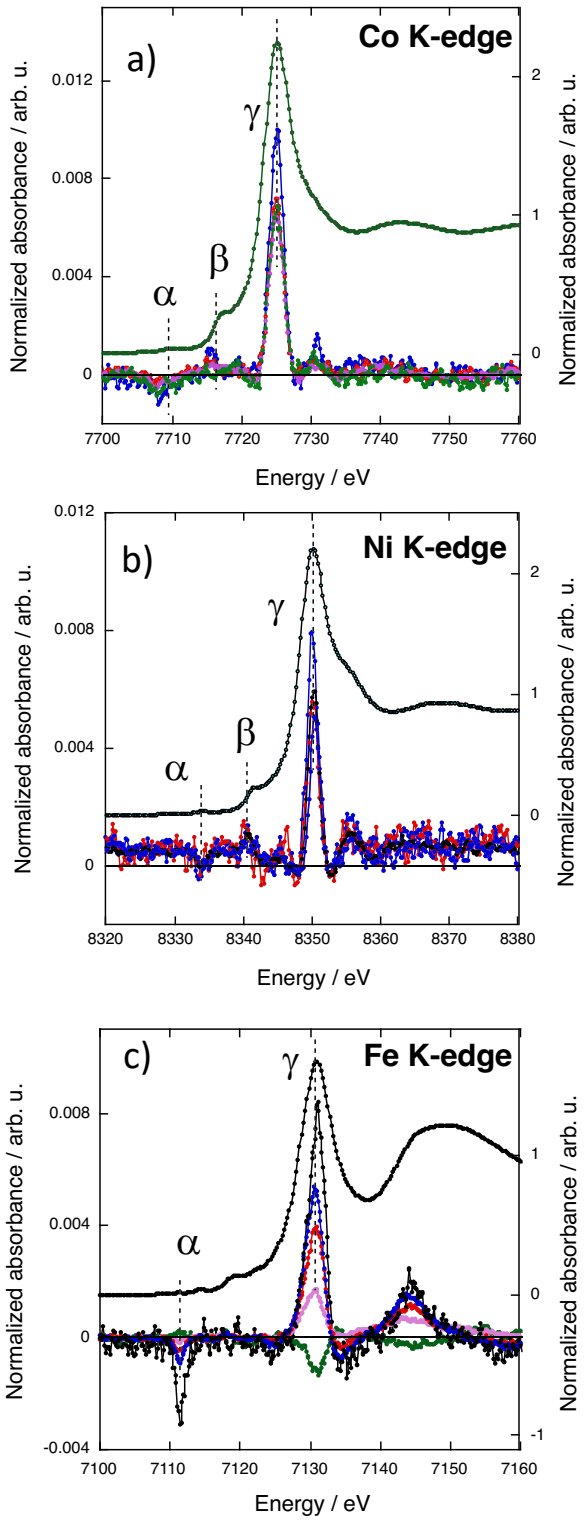

Figure 4. *XMCD signal of* ***CoFe*** *(green),* ***$Co_{0.7}Ni_{0.3}Fe$*** *(pink),* ***$Co_{0.56}Ni_{0.44}Fe$*** *(red),* ***$Co_{0.35}Ni_{0.65}Fe$*** *(blue),* ***NiFe*** *(black) a) at the Co K-edge, b) at the Ni K-edge and c) at the Fe K-edge.*

The Co and Ni ions occupy the same site of the fcc PBA structure, called A site above and in ref. 37. For this A site, the contributions to the signal over the edge and pre-edge regions were already assigned and discussed in ref. 37 and 39. For all compounds, over the pre-edge and edge regions, the XMCD signal exhibit one main contribution (γ) and two other contributions of significantly smaller intensity (α and β), all situated at the same energies along the series. The α contribution can be assigned to the electric-dipole forbidden 1s → 3d transitions and explained by the low symmetry of the site and associated 3d-4p orbital mixing. The β contribution can be assigned to the 1s → $t_{1u}CN\pi^*$ transitions. These two latter contributions will not be further discussed here. The main contribution to the XMCD signal (γ) at the Co K-edge (Figure 4a) and at the Ni K-edge (Figure 4b) can be assigned to the electric-dipole allowed 1s → 4p transitions. For one given K-edge, its intensity is very close from one compound to the other and very close to that of the corresponding bimetallic PBA, except the one of **$Co_{0.35}Ni_{0.65}Fe$**, which is significantly higher at both edges (blue curves). It is now well established that the sign of the main contribution to the XMCD signal in PBAs is directly related to the nature of the exchange interaction between the TM, *i.e.* to the direction of the magnetic moment of the probed atom with regard to the applied magnetic field.[18, 31, 32, 37, 39] The same sign and the same intensity of the main contribution for **CoFe**, **$Co_{0.7}Ni_{0.3}Fe$** and **$Co_{0.56}Ni_{0.44}Fe$** at the Co K-edge on the one hand and for **NiFe**, **$Co_{0.7}Ni_{0.3}Fe$** and **$Co_{0.56}Ni_{0.44}Fe$** at the Ni K-edge on the other hand shows that the magnetic moment borne by the Co(Ni) ions as well as its direction is the same as that of the Co(Ni) ion in the corresponding bimetallic PBA, in line with the magnetic data. One can therefore conclude that, as in the corresponding bimetallic PBA, the magnetic moment of the Co(Ni) ions is aligned in the direction of the magnetic field.

The intensity of the main contribution to the XMCD signal of **$Co_{0.35}Ni_{0.65}Fe$** is significantly higher (25-30%) than that of all other compounds at both the Co and Ni K-edges. This different behavior of **$Co_{0.35}Ni_{0.65}Fe$** arises from different local features of the Co and Ni ions in this compound. The magnetic measurements do not reveal neither a different electronic structure of the Co^{2+} and Ni^{2+} ions in **$Co_{0.35}Ni_{0.65}Fe$** nor a discontinuity in the macroscopic magnetic properties for this compound along the series. Nevertheless, structural strains and slight distortions of the ions' coordination sphere could arise from the different size of the Co^{2+} and Ni^{2+} ions associated in the same A site of the PBA structure. The XRD patterns (S1) show that all compounds crystallize with the same fcc PBA structure, only the lattice constant varies. The variation of the lattice constant value with the percentage of Co^{2+} ions in the A site (Co%) is shown in Figure S4. The lattice constant varies linearly with Co% for **CoFe**, **$Co_{0.70}Ni_{0.30}Fe$** and **$Co_{0.56}Ni_{0.44}Fe$**, indicative that up to the replacement of 44% of Co^{2+} ions by smaller Ni^{2+} ones, the PBA structure accommodates both ions by a decrease of the lattice constant. Nevertheless, one can also see that the lattice constant of **NiFe** departs from this linear variation as well as that of **$Co_{0.35}Ni_{0.65}Fe$**. When the Co% reaches a certain threshold comprised between 56 and 35%, the replacement of Co^{2+} ions by Ni^{2+} ones can no more be compensated by a single

lattice constant decrease. The size of both cations being different, one too small (Ni^{2+}) and the other one too large (Co^{2+}) for the ideal face centered cubic lattice, the structural distortion would be local and different for both ions. Network strains likely develop, slightly distorting the coordination spheres of the Co^{2+} and Ni^{2+} ions and enhancing the departure from the pure O_h symmetry of the local structure of the ions either with a slight displacement of the ion from the crystallographic site and/or a slight tilt of the coordination polymer. Such a local distortion of the A site, by reinforcing the intra-site 3d-4p orbital mixing, could explain the higher intensity of the main contribution to the XMCD signal of **$Co_{0.35}Ni_{0.65}Fe$** at the Co and Ni K-edge.

XMCD at the Fe K-edge.

The XMCD signals of the **$Co_xNi_{(1-x)}Fe$** series at the Fe K-edge are shown in Figure 4c. All the spectra exhibit the same contributions. Over the pre-edge and edge regions, the α and γ contributions can be assigned to the 1s $\rightarrow$ 3d and the 1s $\rightarrow$ 4p transitions respectively.[39] It is striking that the intensity of the γ contribution at the Fe K-edge varies strongly with the Co%. We already showed in ref 39 that the γ contribution at the TM K-edge at the B site is sensitive to the nature of the ion in the A site, on the contrary to the A site which is not sensitive to the ions in the B site ; this difference between both sites is explained by the different symmetries of the sites.[39] In reference 39, we showed that the intensity of the main contribution to the XMCD signal at the Fe K-edge is well reproduced by Eq. 2.

$$I^{Fe} = (1 \pm S_A) * (1/3) * P_{exp} \qquad (2)$$

where S_A is the total spin quantum number of the ion in the A site, the sign in front of S_A depends on the nature of the exchange interaction between the Fe ion and the TM ion in the A site (-(+) for an antiferromagnetic(ferromagnetic) exchange interaction) and P_{exp} is a constant, which depends on the experimental conditions (temperature, magnetic field, circular polarization rate of light). In our experimental conditions, P_{exp} is equal to 0.012.[37, 39] Eq. 2, in which $\pm S_A$ is replaced by $((1-x)S_{Ni} - xS_{Co})$ is given by Eq. 3.

$$I^{Fe} = (1 + (1 - x)S_{Ni} - xS_{Co}) * (1/3) * P_{exp} \qquad (3)$$

Eq. 3 has been used to predict the experimental intensity of the γ peak for our **$Co_xNi_{(1-x)}Fe$** series. The plot of the experimental (I_{exp}) versus the calculated (I_{calc}) intensity using Eq. 3 is shown in Figure 5, where is also reported the plot of I_{exp} versus I_{calc} for the sixteen XMCD signals of the **AFe** PBAs (A^{2+}=Cu^{2+}, Ni^{2+}, Co^{2+}, Mn^{2+}) and the **ACr** PBAs (A^{2+}=Ni^{2+}, Co^{2+},Fe^{2+} , Mn^{2+}) previously investigated and using the expressions for I_{calc} proposed in ref 37 and 39. Figure 5 shows that the experimental intensity of the γ peak at the Fe K-edge is well reproduced by Eq. 3 for all compounds of the **$Co_xNi_{(1-x)}Fe$** series. This result shows that the behaviour of the Fe^{3+} ion magnetic moment in the trimetallic compounds is the same as the latter in the extreme bimetallic compounds (**CoFe** and **NiFe**) weighted by the amount of Co^{2+} and Ni^{2+} ions ; it is antiferromagnetically coupled with the Co^{2+} ions and ferromagnetically coupled with the Ni^{2+} ones, resulting in the distribution of its magnetic moment over the two orientations weighted by the percentage of both Co^{2+} and Ni^{2+} ions in the compound.

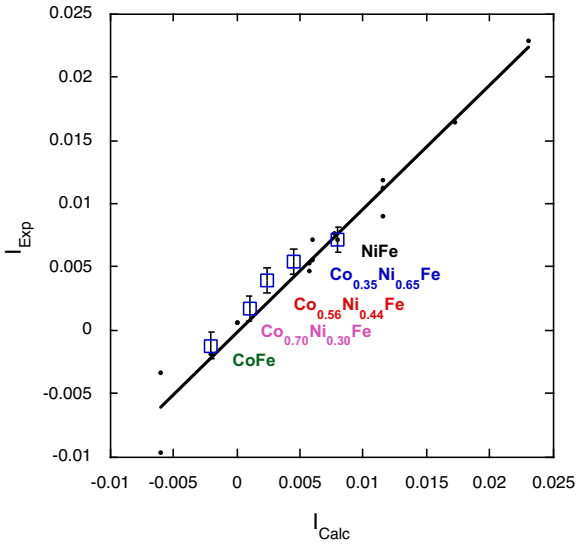

Figure 5. *Experimental (I_{exp}) versus calculated (I_{calc}) intensity using Eq. 3 (blue open squares ; error bar ±0.001) compared to I_{exp} versus I_{calc} for the sixteen XMCD signals of the **AFe** PBAs (A=Cu^{2+}, Ni^{2+}, Co^{2+}, Mn^{2+}) and the **ACr** PBAs (A=Ni^{2+}, Co^{2+},Fe^{2+}, Mn^{2+}) previously investigated in ref. 37 and 39 (black dots).*

Discussion

Input of this work on the understanding of the magnetic properties of PBAs.

The behavior of the magnetic moments carried by all three TM ions (Co^{2+}, Ni^{2+} and Fe^{3+}) can be proposed from the XMCD investigation at the three TM K-edges.

Very close main contributions to the XMCD signal at the Co and Ni K-edges for **$Co_{0.70}Ni_{0.30}Fe$**, **$Co_{0.56}Ni_{0.44}Fe$**, **CoFe** and **NiFe** indicate that the magnetic moments carried by both ions exhibit the same behavior as in the extreme bimetallic compounds **CoFe** and **NiFe**. This means that the magnetic moments of the Co^{2+} and Ni^{2+} ions are aligned in the direction of the applied magnetic field. This is in agreement with the experimental values of the magnetization at 4T, significantly higher than those calculated using Eq. 1 considering antiparallel magnetic moments for the Co^{2+} and Ni^{2+} ions, as was the case for the Mn^{2+} and Ni^{2+} ions along the **$Mn_xNi_{(1-x)}Cr$** series in ref. 40-43. The magnetic moments really borne by the Co^{2+} and Ni^{2+} ions are schematized as plain blue and plain green arrows in Figure 6.

In the case of the Fe K-edge, the variation of the intensity of the main contribution to the XMCD signal is well reproduced by Eq. 3. As mentioned above, this suggests that the behaviour of the Fe^{3+} ion magnetic moment in the trimetallic compounds is the same as that of the latter in the extreme bimetallic compounds,

antiferromagnetically coupled with the Co^{2+} ions and ferromagnetically coupled with the Ni^{2+} ones but weighted by the amount of Co^{2+} and Ni^{2+} ions in the compounds.

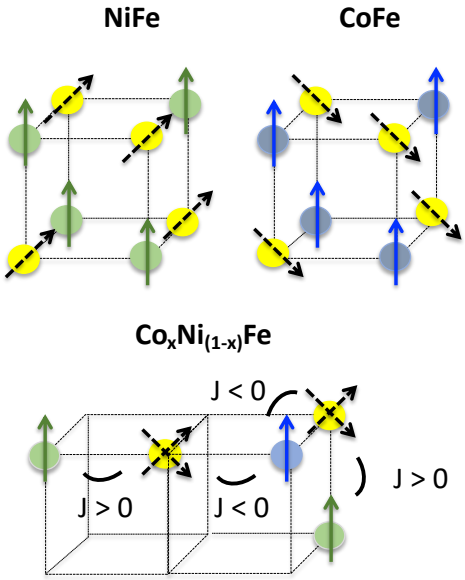

Figure 6. *Scheme of the proposed orientations of the magnetic moments for an octant of the fcc PBA structure. The Ni^{2+}, Co^{2+} and Fe^{3+} ions are represented by green, blue and yellow sphere respectively and their magnetic moments by plain green, plain blue and dotted black arrows. The orientation of the magnetic moment with regard to the crystallographic axes are those proposed in ref. 39. The proposed alignment of the Fe magnetic moments along the <111> directions is in line with a slight trigonal distortion of the $Fe(CN)_6$ entities[54] and a strong spin-orbit coupling.*

Such a magnetic situation could lead to spin frustration in the PBAs, especially since **NiFe** and **CoFe** present close strength of exchange interactions between both pairs of ions.[‡,52] A frustration parameter given by $f = |\theta|/T_{C/N}$ has been introduced to evaluate the frustration degree and the condition $|\theta|/T_{C/N} > 10$ has been proposed as a criterion for the presence of frustration.[53] Along the **Co$_x$Ni$_{(1-x)}$Fe** series, the linear variation of θ with x (Figure S5), the low value of the f parameter ($f < 1.5$) for all compounds, the classical profile of the FC and ZFC magnetization curves, as well as the orientation of each pair of spins consistent with the sign of the corresponding J constant, allow us to rule out the presence of spin frustration in the compounds of the series, as it was the case for the **Mn$_x$Ni$_{(1-x)}$Cr** series previously studied.[40] From the variation of the intensity of the Fe K-edge XMCD signal (Eq. 3) along the **Co$_x$Ni$_{(1-x)}$Fe** series, we propose an orientation of the magnetic moments carried by the Fe^{3+} ions with regard to that of the applied magnetic field dictated by the weighted amount of both the Ni^{2+} and Co^{2+} ions in the A sub-lattice, without spin frustration. The direction and orientation of the magnetic moment borne by the Fe^{3+} ions under the influence of Co^{2+} or Ni^{2+} ions are schematized as black doted arrows in Figure 6.

The main difference between the comparable **Mn$_x$Ni$_{(1-x)}$Cr** PBA series and our **Co$_x$Ni$_{(1-x)}$Fe** series is that, in the former, the orientation of the magnetic moments at low temperature is directly dictated by the exchange interaction between each ions pair (Ni-Cr and Mn-Cr). On the contrary, in our series the magnetic moments of the Co^{2+} and Ni^{2+} ions at the A site both align in the direction of the magnetic field despite the different nature of exchange interactions with the Fe^{3+} ion that they surround, and then, the orientation of the magnetic moment carried by the Fe^{3+} ions is dictated by the exchange interactions between the ions' pairs (Ni-Fe and Co-Fe), the average orientation being dictated by the relative amount of both Co^{2+} and Ni^{2+} ions. These different magnetic behaviors of the **Mn$_x$Ni$_{(1-x)}$Cr** and **Co$_x$Ni$_{(1-x)}$Fe** PBA series arise from different magnetic behaviors of the TM ions listed below. First, due to the higher number of unpaired electrons in the t_{2g} orbitals for the Cr^{3+} ions (3 against 1 for the Fe^{3+} ions), the exchange interactions with the surrounding ions (Mn^{2+} and Ni^{2+}) are stronger in the **Mn$_x$Ni$_{(1-x)}$Cr** series than in the **Co$_x$Ni$_{(1-x)}$Fe** series. Second, due to slight different geometry of the $M(CN)_6$ entities, octahedral for $Cr(CN)_6$ and slightly trigonally distorted for $Fe(CN)_6$ with strong spin-orbit coupling (see above and reference 39), the directions of the magnetic moments borne by the TM ion in these entities is different: aligned along the same <100> directions as those of the TM ions on the A site for the $Cr(CN)_6$ entities, while for the $Fe(CN)_6$ entities aligned along the <111> directions, different from those of the magnetic moments carried by the ions on the A site. Third, ref. 55 showing a comparable behavior for the $Cu_{0.73}Mn_{0.77}[Fe(CN)_6]\bullet zH_2O$ compound as those of the **Mn$_x$Ni$_{(1-x)}$Cr** series, a stronger magnetic anisotropy of the Co^{2+} and Ni^{2+} ions in the **Co$_x$Ni$_{(1-x)}$Fe** series than that of the Mn^{2+} and Ni^{2+} ions in the **Mn$_x$Ni$_{(1-x)}$Cr** series can also be mentioned.[39] At last, one can also not exclude a role of the exchange interactions between TM second neighbors more important than considered so far.

Input of this work on the understanding of XMCD at the transition metal K-edge for the study of molecular materials.

1. Probed species.

In a previous work,[37] we showed that the features of the main contribution to the XMCD signal at the TM K-edge of TM ions at the A site for the two **AFe** (A^{2+}=Cu^{2+}, Ni^{2+}, Co^{2+}, Mn^{2+}) and **ACr** (A^{2+}=Ni^{2+}, Co^{2+},Fe^{2+} , Mn^{2+}) PBAs series i) do not depend on the nature of the TM ion at the B site and ii) can be related to the electronic structure and magnetic behavior of the A^{2+} ion or of the A^{2+} ions sublattice : the shape of the signal to the filling of the 3d orbitals, the sign of the signal to the orientation of the magnetic moment with regard to that of the applied magnetic field; we also proposed an expression of its intensity as a function of the total spin quantum number S_A. The present study confirms the previous results and allows us to go a bit further concerning the species probed by XMCD at the A site of PBAs. As the intensity of the 1s $\rightarrow$ 4p XMCD contribution of **CoFe** at the Co K-edge is different from the one of **NiFe** at the Ni K-edge, the very close XMCD signals for the majority of the **Co$_x$Ni$_{(1-x)}$Fe** series at the Co(Ni) K-edge show that the 1s $\rightarrow$ 4p contribution to the XMCD signal at the K-edge of the ions on the

A site is sensitive neither to the replacement of one ion by the other in the A ions sublattice nor to the average distance between the same ions of the A ions sublattice. Hence, XMCD at the K-edge of TM ions on the A site of the molecular PBA compounds is not a probe of the sublattice or of a part of the sublattice of the ions on the A site. In that case, the contribution to the signal of each absorbing atom, encompassing either the contribution of all other ions of the sublattice (overlap of all 4p orbitals of the A^{2+} ions) or the contribution of all other same atoms of the sublattice (overlap of all 4p orbitals of the probed Co^{2+} or Ni^{2+} ions), would vary with the chemical composition of the sublattice, which is not observed. On the contrary, XMCD at the K-edge of TM ions on the A site of the molecular PBA compounds is a local probe of each absorbing atom without any influence from other ions and the XMCD signal at the K-edge of the ions on the A site is the average of all their contributions.

The case of the B site is different because our previous work showed that the 1s → 4p XMCD signal at the K-edge of the ions on the B site of PBAs contains not only information on the ions or the sublattice of the ions on the B site but also on the ions on the A site.[39] In order to determine whether XMCD at the K-edge of ions at the B site of PBAs is a local probe of the ion on the B site and its TM neighbors or a more extended probe, 50% of the $Fe(CN)_6$ entities were replaced by $Cr(CN)_6$ ones in **NiFe**. This compound is called **$NiCr_{0.50}Fe_{0.50}$** in the following and its X-ray diffraction pattern, FC-ZFC magnetization curves and magnetic field dependance of the magnetization at 4K are shown in S6-S8. The XMCD signals of **$NiCr_{0.50}Fe_{0.50}$** were compared to those of **NiFe** and the NiCr PBA (called **NiCr**) of chemical formula $Ni_4[Cr(CN)_6]_{8/3}\bullet 17H_2O$, the synthesis and characterization of which are both presented in ref. 37. Figure 7a shows the XMCD signal at the Ni K edge of **NiFe**, **$NiCr_{0.50}Fe_{0.50}$** and **NiCr**. As expected, the signals are the same. XMCD at the TM ion on the A site of PBAs is a local probe of the ion, which is in a very close environment in the three PBAs, with definitely no influence from the TM ions in the B sites. Figures 7b and 7c show the XMCD signals of **$NiCr_{0.50}Fe_{0.50}$** compared to those of **NiCr** at the Cr K-edge and of **NiFe** at the Fe K-edge, respectively. The XMCD signal of **$NiCr_{0.50}Fe_{0.50}$** is the same as that of **NiCr** at the Cr K-edge and the same as that of **NiFe** at the Fe K-edge. This result shows that, as at the K-edge of the TM ions on the A site, XMCD at the K-edge of the TM ions on the B site is not sensitive to the replacement of part of them and is therefore a local probe of the ion at the B site and its first metallic neighbors.

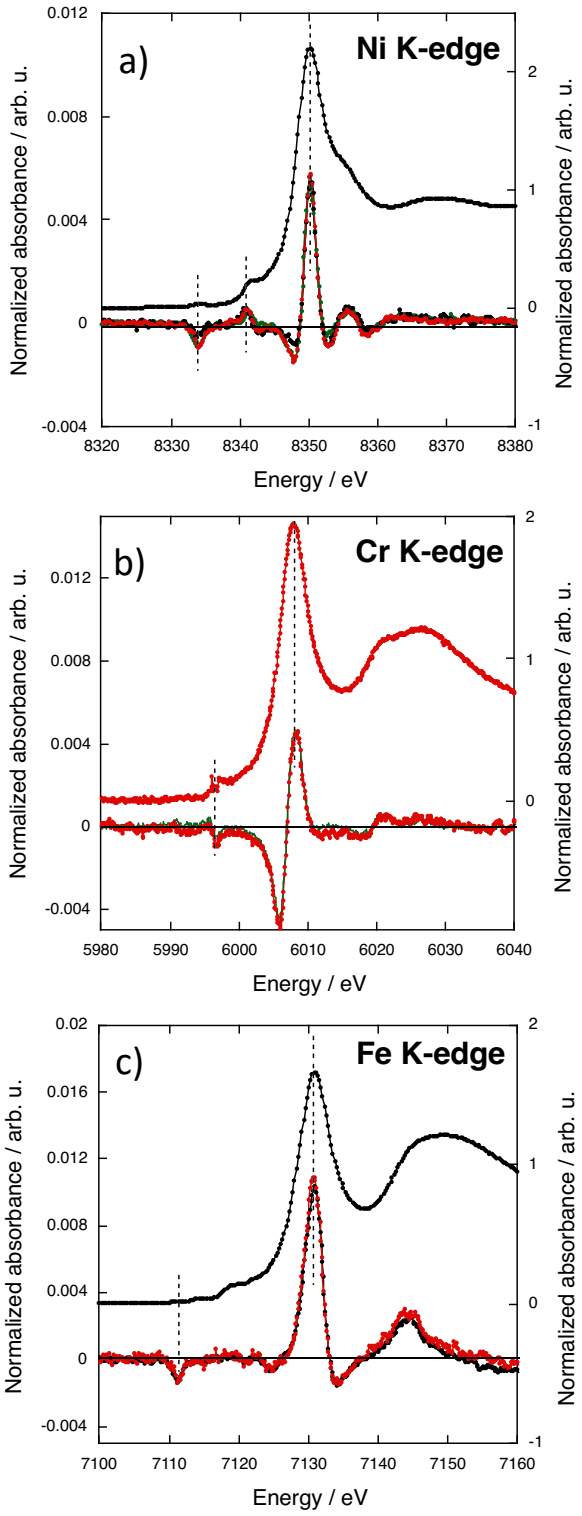

Figure 7. *a) XMCD signal at the Ni-K edge of* ***NiFe*** *(black),* ***$NiCr_{0.50}Fe_{0.50}$*** *(red) and* ***NiCr*** *(green) and XANES at the Ni K-edge of* ***NiFe*** *(black) ; b) XMCD signal at the Cr K-edge of* ***$NiCr_{0.50}Fe_{0.50}$*** *(red) and* ***NiCr*** *(green) and XANES at the Cr K-edge of* ***$NiCr_{0.50}Fe_{0.50}$*** *(red) ; c) XMCD signal at the Fe K-edge of* ***$NiCr_{0.50}Fe_{0.50}$*** *(red) and* ***NiFe*** *(black) and XANES at the Fe K-edge of* ***NiFe*** *(black).*

2. XMCD at the TM K-edge, a probe extremely sensitive to very slight structural distortions.

Variable pressure XMCD measurements at the Ni and Fe K-edges of NiFe at 4 K already showed that XMCD at the TM K-edge is very sensitive to slight structural distortions.[18] This high sensitivity arises from the symmetry dependent mixing of the 3d and 4p orbitals. As discussed above, the higher intensity of the 1s → 4p XMCD signal at the Co and Ni K-edges of $Co_{0.35}Ni_{0.65}Fe$ can be assigned to a slight distortion of the Co and the Ni sites due to network strains arising from the accommodation of ions of different sizes in the same sublattice of the PBA. No such effect is observed at the Fe K-edge of this compound. This is expected as the $Fe(CN)_6$ entity, in which the Fe^{3+} ion is low spin, is made of stronger and more covalent bonds than the Co^{2+} and Ni^{2+} high spin-to-ligands bonds. X-ray Absorption Near Edge Spectra (XANES) is a probe of the local structure around the absorbing atom. The XANES spectra of **$Co_{0.35}Ni_{0.65}Fe$** was recorded at the Co, Ni and Fe K-edges and compared to those of **CoFe** and **NiFe**; they are shown in Figure 8. Figure 8 shows that, whatever the K-edge, the XANES spectra of **$Co_{0.35}Ni_{0.65}Fe$** is very close to those of **CoFe** and of **NiFe**. The distortion of the Co^{2+} and Ni^{2+} sites is probably too small to be detectable on the XANES spectra at the TM K-edge. This therefore shows that XMCD at the TM K-edge could turn out to be an unprecedented tool to detect and analyze very slight distortions affecting magnetic sites.

Experimental

One series of five $(Co_xNi_{(1-x)})_4[Fe(CN)_6]_{8/3}\bullet nH_2O$ PBAs (called **$Co_xNi_{(1-x)}Fe$**) was synthesized. EDS analyses, powder X-ray diffraction and magnetic measurements were performed using the devices of the ICMMO instrumentation platform. The syntheses and characterizations of the two extreme compounds **CoFe** and **NiFe** were presented in ref. 37.

Sample preparation.

The three PBAs were synthesized by a drop-by-drop addition of two precursors in aqueous solutions: a 400 mL aqueous solution of potassium hexacyanoferrate(III) $K_3[Fe(CN)_6]$ (c = $2.5.10^{-3}$ mol.L^{-1}) was added to a 100 mL aqueous solution of a mixture of $Co(NO_3)_2$ and $Ni(NO_3)_2$ salts (c_{tot} = 50.10^{-3} mol.L^{-1}). The precipitates were washed with distilled water and centrifuged three times at 8000 rpm, and finally allowed to dry in air at room temperature.

Energy Dispersive Spectroscopy (EDS) analyses.

The chemical formulas of the three trimetallic PBAs were determined by EDS analyses, using an EDS spectrometer installed on a ZEISS Sigma HD microscope. Data processing was done using the IDFix EDS analysis software. The results are given in S1 for the **$Co_xNi_{(1-x)}Fe$** series.

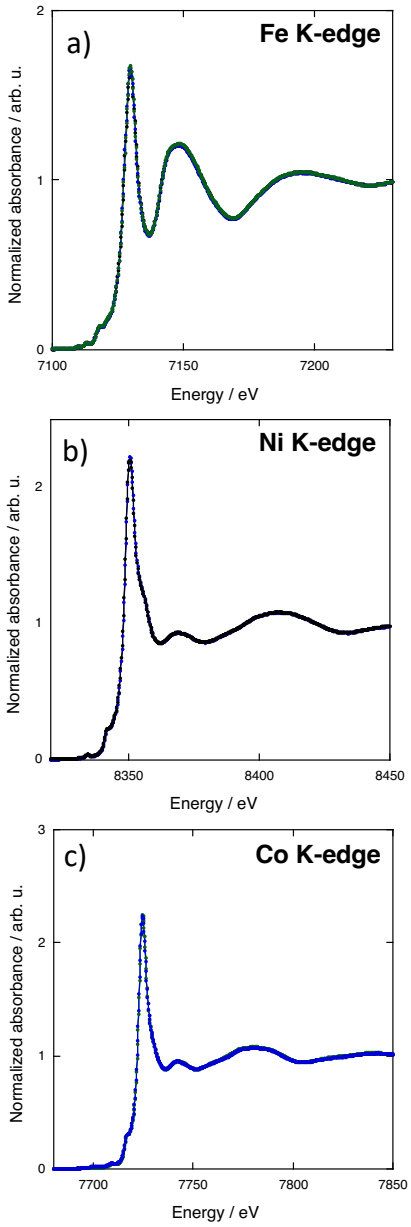

Figure 8. *a) XANES spectra at the Fe K-edge of* ***$Co_{0.35}Ni_{0.65}Fe$*** (blue), ***CoFe*** *(green) and* ***NiFe*** *(black); b) XANES spectra at the Ni K-edge of* ***$Co_{0.35}Ni_{0.65}Fe$*** (blue) and ***NiFe*** *(black) c) XANES spectra at the Co K-edge of* ***$Co_{0.35}Ni_{0.65}Fe$*** *(blue)* and ***CoFe*** *(green).*

Powder X-Ray Diffraction (XRD).

Powder XRD data were collected with a Philips X'Pert diffractometer (Cu $K\alpha_1$ radiation) at room temperature. All diagrams were recorded over the 10-70° 2θ angle range with steps of 0.01°. An aluminum sample holder was used for all measurements. The cell parameters were extracted by a Lebail refinement procedure (using the Fullprof software), considering a Fm3m space group. The XRD patterns and corresponding cell parameters for the **$Co_xNi_{(1-x)}Fe$** series are given in S1.

SQUID magnetometry.

Magnetic properties were investigated using a Quantum Device XL-7 SQUID magnetometer. 5.6 mg of PBA powder was placed in a capsule and 17 mg of eicosane were added to ensure that the particles would not move with the application of the magnetic field. Field Cooled-Zero Field Cooled (FC-ZFC) measurements were performed over the 2K-100K temperature range under a 30 Oe magnetic field (S2). In order to determine the Weiss temperature (θ), the magnetization was measured as a function of temperature up to 300K under a 5000 Oe magnetic field; the experimental curves were fitted using a Curie-Weiss law (S3). Finally, the magnetic field dependence of magnetization was recorded at 4K for a magnetic field varying between -40000 Oe (-4 T) and 40000 Oe (4 T).

Transition metal K-edge XAS.

X-ray Absorption spectra in the transmission mode were recorded for the **$Co_xNi_{(1-x)}Fe$** series at the three K-edges on the SAMBA beamline[56] at SOLEIL (Gif sur Yvette, France). We used a Si(220) monochromator and recorded the spectra in a continuous mode. Measurements were performed at room temperature on pellets. We carefully checked that no radiation damage occurred. Following the measurements, the spectra were energy-calibrated and conventionally normalized using the ATHENA software.[57]

TM K-edge XMCD.

Co, Ni and Fe K-edges X-ray Absorption Near-Edge Structure (XANES) spectra and XMCD signals were recorded in the transmission mode using the dispersive setup of the ODE beamline[58, 59] at SOLEIL synchrotron (Gif sur Yvette, France). Detailed information is given about the measurements and normalization procedure in Ref 36, so only the main ones are reminded here. The circular polarization rate is the same for all the edges. The Si(311) polychromator was chosen to reach the highest possible resolution in the white line region of the spectra. Then, it is critical (i) to be well below the Curie temperature of the eight investigated PBAs, and (ii) to avoid any artifact in the intensity related to a change in the temperature, so we were careful to perform the measurements at 4K. The largest external magnetic field (1.3T) that can be reached when the cryostat is used was applied alternatively parallel and antiparallel to the direction of the photon beam. The samples were placed in a Diamond Anvil Cell (DAC) and, to minimize the absorption of the beam while retaining a brilliant enough flux to be able to perform the measurements, the diamonds of the DAC were replaced by Plexiglas strips. No radiation damage occurred thanks to attenuators of appropriate thickness. A metallic foil was recorded at both edges for energy calibration. We normalized the XANES spectra and XMCD signals using the procedure described in ref. 36.

Conclusions

The study of the trimetallic **$Co_xNi_{(1-x)}Fe$** PBA series by TM K-edge XMCD at the Co, Ni and Fe K-edges shows that XMCD is i) a fruitful local and quantitative probe of the magnetic moment carried by the TM ions in PBAs as well as ii) an extremely sensitive probe to slight structural distortions. In transmission mode, the whole sample is probed, and the local picture obtained at each K-edge nicely completes the macroscopic magnetic data, allowing for a deeper insight into the magnetic and structural behavior of each sample.

In return, the use of the trimetallic **$Co_xNi_{(1-x)}Fe$** PBA series as a tool to better understand the TM K-edge XMCD in PBAs allows for the evaluation of the nature of the probed species. Thus, the effect of the partial replacement of one TM ion by another in both sub-lattices clearly shows that TM K-edge XMCD is a strictly local probe. At the A site, TM K-edge XMCD is an atomic probe of only the probed element. At the B site, due to the departure from centro-symmetry of the A site and the associated 3d-4p mixing,[39] XMCD at the TM K-edge is a local probe of the probed element but also of its first magnetic neighbors. At last, XMCD at the TM K-edge is highly sensitive to very small structural distortion undetectable or hardly detectable by X-ray absorption spectroscopy. TM K-edge XMCD can therefore nicely complement X-ray absorption spectroscopic investigations when slight structural distortions are at play and could turn out to be an unprecedented tool to detect and analyze very slight distortions affecting magnetic sites.

The Prussian blue analogues have been chosen as model compounds to better understand TM K-edge XMCD, because some electronic and structural parameters can be selectively varied and were successfully related to XMCD features. One next step will be to extend the interpretation of the TM K-edge XMCD signals of PBAs to i) other molecular magnetic materials and to ii) materials, the electronic structure of which is well-described in terms of molecular orbitals. Another step will be to get direct experimental evidence of our hypothesis on the relative orientation of the magnetic moments and crystallographic axes (ref. 37, ref. 39, this work). Resonant X-ray scattering using circularly polarized X-rays or neutron diffraction could be performed to get such evidence.

Author Contributions

The authors are sad to specify that their colleague, co-author and friend, François Baudelet, passed on January 28th, 2022. He carried out the experiments during two synchrotron beamtimes for the results presented here and was deeply involved in the interpretation of the data.

The manuscript was written through the contribution of all other authors, who have given approval to the final version of the manuscript.

Conflicts of interest

There are no conflicts to declare.

Acknowledgements

Financial support was provided for the whole TM K-edge XMCD project and the Ph.D. grant of A. N'Diaye by ANR MagDiDi (ANR-

17-CE29-0011), Paris-Saclay University and the CNRS. The authors acknowledge SOLEIL for the provision of synchrotron radiation facility on the ODE beamline through proposals 20190412 and 20201335 on the SAMBA beamline through proposal 20180264.

Notes and references

‡ The absolute value of the ratio between the magnetic coupling constant between both **NiFe** (J_{NiFe}) and **CoFe** (J_{CoFe}) ions pairs can be estimated within the mean-field approach by considering dominant exchange interaction between neighboring TM ions.[52] Indeed, the proportional relationship between $T_{C/N}$, the magnetic ordering temperature, z the number of magnetic neighbors and J the magnetic coupling constant for a given PBA is given by: $T_{C/N} \propto zJ$. The number of magnetic neighbors being the same in **NiFe** and **CoFe**, this approximation gives the value of 1.6 for $|J_{NiFe}/J_{CoFe}|$, indicative of exchange interactions with close strengths between both pairs of ions. Such close strength of exchange interactions of different nature in the same PBA network could give rise to spin frustration.

1 B. T. Thole, P. Carra, F. Sette and G. van der Laan, *Phys. Rev. Lett.*, 1992, **68**, 1943.
2 P. Carra, B. T. Thole, M. Altarelli and X. Wang, *Phys. Rev. Lett.*, 1993, **70***,* 694.
3 C. T. Chen, Y.U. Idzerda, H.-J. Lin, N. V. Smith, G. Meigs, E. Chaban, G. H. Ho, E. Pellegrin and F. Sette, *Phys. Rev. Lett.*, 1995, **75**, 152.
4 R. Moroni, C. Cartier dit Moulin, G. Champion, M.-A. Arrio, Ph. Sainctavit, M. Verdaguer and D. Gatteschi, *Phys. Rev. B*, 2003, **68**, 064407.
5 A. Rogalev and F. Wilhelm, *Phys. Metals Metallography*, 2015, **116**, 1285.
6 J. I. Igarashi and K. Hirai, *Phys. Rev. B*, 1996, **53**, 6442.
7 N. Bouldi, N. J. Vollmers, C. G. Delpy-Laplanche, Y. Joly, A. Juhin, Ph. Sainctavit, Ch. Brouder, M. Calandra, L. Paulatto, F. Mauri and U. Gerstmann, *Phys. Rev. B*, 2017, **96***,* 085123.
8 H. Ebert, *Solid State Commun.*, 1996, **100**, 677.
9 S. Stähler, G. Schütz and H. Ebert, *Phys. Rev. B*, 1993, **47**, 818.
10 H. J. Gotsis and P. A Strange, *J. Phys. Condens. Matter*, 1994, **6**, 1409.
11 G. Y. Guo, *J. Phys. Condens. Matter*, 1996, **8**, L747.
12 Ch. Brouder and M. Hikam, *Phys. Rev. B*, 1991, **43**, 3809.
13 Ch. Brouder, M. Alouani and K. H. Bennemann, *Phys. Rev. B*, 1996, **54**, 7334.
14 C. R. Natoli, M. Benfatto and S. Doniach, *Phys. Rev. A*, 1986, **34**, 4682.
15 Y. Joly, O. Bunau, J. E. Lorenzo, R. M. Galéra, S. Grenier and B. Thompson, *J. Phys. Conf. Ser.*, 2009, **190**, 012007.
16 R. Torchio, O. Mathon and S. Pascarelli, *Coord. Chem. Rev.*, 2014, **277–278**, 80.
17 F. Baudelet, S. Pascarelli, O. Mathon, J.-P. Itié, A. Polian, M. d'Astuto and J.-C. Chervin, *J. Phys. Condens. Matter*, 2005, *17*, S957.
18 J.-D. Cafun, J. Lejeune, J.-P. Itié, F. Baudelet and A. Bleuzen, *J. Phys. Chem. C*, 2013, **117**, 19645.
19 N. Ishimatsu, T. Shichijo, Y. Matsushima, H. Maruyama, Y. Matsuura, T. Tsumuraya, T. Shishidou, T. Oguchi, N. Kawamura, M. Mizumaki, T. Matsuoka and K. Takemura, *Phys. Rev. B*, 2012, **86**, 104430.
20 R. Torchio, Y. O. Kvashnin, S. Pascarelli, O. Mathon, C. Marini, L. Genovese, P. Bruno, G. Garbarino, A. Dewaele, F. Occelli and P. Loubeyre, *Phys. Rev. Lett*, 2011, **107**, 237202.
21 R. Torchio, A. Monza, F. Baudelet, S. Pascarelli, O. Mathon, E. Pugh, D. Antonangeli and J.-P. Itié, *Phys. Rev. B*, 2011, **84**, 060403(R).
22 G. Schütz, W. Wagner, W. Wilhelm, P. Kienle, R. Zeller, R. Frahm and G. Materlik, *Phys. Rev. Lett.*, 1987, **58**, 737.
23 G. van der Laan, B. T. Thole, G. A. Sawatzky, J. B. Goedkoop, J. C. Fuggle, J.-M. Esteva, R. C. Karnatak, J. P. Remaika, H. A. Dabkowska, *Phys. Rev. B*, 1986, **34**, 6529.
24 J. P. Rueff, R. M. Galéra, Ch.Giorgetti, E. Dartyge, Ch. Brouder and M. Alouani, *Phys. Rev. B*, 1998, **58**, 12271.
25 J. Herrero-Albillos, F. Bartolomé, L. M. Garcia, P. Cerbuna, F. Casanova, A. Labarta and X. Batlle, *Phys. Rev. B*, 2007, **75**, 187402.
26 M. A. Laguna-Marco, C. Piquer and J. Chaboy, *Phys. Rev. B*, 2009, **80**, 144419.
27 V. Gadet, T. Mallah, I. Castro, M. Verdaguer and P. Veillet, *J. Am. Chem. Soc.*, 1992, **114**, 9213.
28 T. Mallah, S. Thiébaut, M. Verdaguer and P. Veillet, *Science*, 1993, **262**, 1554.
29 S. Ferlay, T. Mallah, R. Ouahès, P. Veillet and M. Verdaguer, *Nature*, 1995, **378**, 701.
30 T. Mallah, S. Ferlay, C. Auberger, C. Hélary, F. L'Hermite, R. Ouahès, J. Vaissermann, M. Verdaguer and P. Veillet, *Mol. Cryst. Liq. Cryst.*, 1995, **273**, 141.
31 M. Verdaguer, T. Mallah, C. Hélary, F. L'Hermite, P. Sainctavit, M.-A. Arrio, D. Babel, F. Baudelet, E. Dartyge and A. Fontaine, *Physica B*, 1995, **208–209**, 765.
32 E. Dujardin, S. Ferlay, X. Phan, C. Desplanches, C. Cartier dit Moulin, P. Sainctavit, F. Baudelet, E. Dartyge, P. Veillet and M. Verdaguer, *J. Am. Chem. Soc.*, 1998, **120**, 11347.
33 J. M. Herrera, A. Bachschmidt, F. Villain, A. Bleuzen, V. Marvaud, W. Wernsdorfer and M. Verdaguer, *Phil. Trans. R. Soc. A*, 2008, **366**, 127.
34 G. Champion, V. Escax, C. Cartier dit Moulin, A. Bleuzen, F. Villain, F. Baudelet, E. Dartyge and M. Verdaguer, *J. Am. Chem. Soc.*, 2001, **123**, 12544.
35 A. Bordage, L. Nataf, F. Baudelet and A. Bleuzen, *J. Phys.: Conf. Series*, 2016, **712**, 012109.
36 A. N'Diaye, A. Bordage, L. Nataf, F. Baudelet, T. Moreno and A. Bleuzen, *J. Synchrotron Rad.,* 2021, **28***,* 1127.
37 A. N'Diaye, A. Bordage, L. Nataf, F. Baudelet, E. Rivière and A. Bleuzen, *Inorg. Chem.,* 2022, **61**, 6326.
38 A. Bordage, A. N'Diaye and A. Bleuzen, *C. R. Chimie*, 2022*,* **25**, 281.
39 A. N'Diaye, A. Bordage, L. Nataf, F. Baudelet, E. Rivière and A. Bleuzen, *ACS Omega,* 2022, **7**, 36366.
40 S.-I. Ohkoshi, T. Iyoda, A. Fujishima and K. Hashimoto, *Phys. Rev. B*, 1997, **56**, 11642.
41 S.-I. Ohkoshi, O. Sato, T. Iyoda, A. Fujishima and K. Hashimoto, *Inorg. Chem.*, 1997, **36**, 268.
42 S.-I. Ohkoshi, S. Yorozu, O. Sato, T. Iyoda, A. Fujishima and K. Hashimoto, *Appl. Phys. Lett.*, 1997, **70**, 1040.
43 S.-I. Ohkoshi, O. Sato, A. Fujishima and K. Hashimoto, *J. Am. Chem. Soc.*, 1998, **120**, 5349.
44 S.-I. Ohkoshi and K. Hashimoto, *Phys. Rev. B*, 1999, **60**, 12820.
45 S.-I. Ohkoshi and K. Hashimoto, *J. Am. Chem. Soc.*, 1999, **121**, 10591.
46 A. Widmann, H. Kahlert, I. Petrovic-Prelevic, H. Wulff, J. V. Yakhmi, N. Bagkar and F. Scholz, *Inorg. Chem.*, 2002, **41**, 5706.
47 A. Kumar and S.M. Yusuf, *Physica B*, 2005, **362**, 278.
48 L. Egan, K. Kamenev, D. Papanikolaou, Y. Takabayashi and S. Margadonna, *J. Am. Chem. Soc.*, 2006, **128**, 6034.
49 D. M. Pajerowski, J. E. Gardner, D. R. Talham and M. W. Meisel, *J. Am. Chem. Soc.*, 2009, **131**, 12927.
50 D. M. Pajerowski, T. Yamamoto and Y. Einaga, *Inorg. Chem.*, 2012, **51**, 3648.

51 F. J. Luque, I. A. Kowalik, J. P. Prieto-Ruiz, M. A. Nino, H. Prima-Garcia, F. M. Romero, D. Arvanitis, E. Coronado, R. Miranda and J. J. de Miguel, J. *Mater. Chem. C*, 2018, **6**, 8171.
52 J.S. Smart, Effective Field Theory of Magnetism, W. B. Saunders Company, Philadelphia and London, 1966.
53 J. E. Greedan, *J. Mater. Chem.*, 2001, **11**, 37.
54 M. Atanasov, P. Comba, C. A. Daul and A. Hauser, *J. Phys. Chem. A*, 2007, **111**, 9145.
55 A. Kumar, S. M. Yusuf, L. Keller and J.V. Yakhmi, *Phys. Rev. Lett.*, 2008, **101**, 207206.
56 V. Briois, E. Fonda, S. Belin, L. Barthe, C. La Fontaine, F. Langlois, M. Ribens and F. Villain, *UVX 2010 EDP Sciences*, 2011, 41.
57 B. Ravel and M. Newville, *J. Synchrotron Rad.*, 2005, **12**, 537.
58 F. Baudelet, Q. Kong, L. Nataf, J.-D. Cafun, A. Congedutti, A. Monza, S. Chagnot and J.-P. Itié, *High Pressure Research* 2011, **31**, 136.
59 F. Baudelet, L. Nataf, R. Torchio, *High Pressure Research* 2016, **36**, 429.

ARTICLE

TOC

The magnetic properties of a series of trimetallic (Co,Ni)Fe PBA were studied at the local and macroscopic scale, bringing new information on TM K-edge XMCD and on the competing exchange interactions between the Co-Fe and Ni-Fe pairs.